Electric propulsion for small satellites

2015 Plasma Phys. Control. Fusion 57 014005

IOP Publishing Plasma Physics and Controlled Fusion
Plasma Phys. Control. Fusion **57** (2015) 014005 (10pp) doi:10.1088/0741-3335/57/1/014005

Electric propulsion for small satellites

Michael Keidar, Taisen Zhuang, Alexey Shashurin, George Teel, Dereck Chiu, Joseph Lukas, Samudra Haque and Lubos Brieda

Mechanical and Aerospace Engineering, The George Washington University, Washington, DC 20052, USA

E-mail: keidar@gwu.edu

Received 1 July 2014, revised 28 August 2014
Accepted for publication 1 September 2014
Published 28 November 2014

Abstract

Propulsion is required for satellite motion in outer space. The displacement of a satellite in space, orbit transfer and its attitude control are the task of space propulsion, which is carried out by rocket engines. Electric propulsion uses electric energy to energize or accelerate the propellant. The electric propulsion, which uses electrical energy to accelerate propellant in the form of plasma, is known as plasma propulsion. Plasma propulsion utilizes the electric energy to first, ionize the propellant and then, deliver energy to the resulting plasma leading to plasma acceleration. Many types of plasma thrusters have been developed over last 50 years. The variety of these devices can be divided into three main categories dependent on the mechanism of acceleration: (i) electrothermal, (ii) electrostatic and (iii) electromagnetic. Recent trends in space exploration associate with the paradigm shift towards small and efficient satellites, or micro- and nano-satellites. A particular example of microthruster considered in this paper is the micro-cathode arc thruster (μCAT). The μCAT is based on vacuum arc discharge. Thrust is produced when the arc discharge erodes some of the cathode at high velocity and is accelerated out the nozzle by a Lorentz force. The thrust amount is controlled by varying the frequency of pulses with demonstrated range to date of 1–50 Hz producing thrust ranging from 1 μN to 0.05 mN.

Keywords: plasma propulsion, micropropulsion, micro-cathode arc thruster

(Some figures may appear in colour only in the online journal)

1. Introduction

Propulsion is required for satellite motion in outer space. The orbit transfer of a satellite, station-keeping and attitude control are performed by utilizing rocket engines. Rocket engines operate according to the basic principle of action and reaction leading to momentum transfer. A force (thrust) F on the spacecraft is formed by ejecting a jet of gas or plasma in the backward direction. In principle, there are two major types of rocket engines, which are distinguished by the energy source used to accelerate the gas, namely chemical and electric rockets. Electric propulsion uses electric energy to energize or accelerate the propellant. The electric propulsion, which uses electrical energy to accelerate propellant in the form of plasma, is known as plasma propulsion. Plasma propulsion utilizes electric energy to first, ionize the propellant, and then, deliver energy to the resulting plasma leading to plasma acceleration.

An important characteristic of the plasma thruster is the total propulsive action on a spacecraft, which is measured by the velocity change. The term delta-V (ΔV) constitutes the sum of all velocity changes by the spacecraft due to thruster operation. In the proximity of large celestial bodies, ΔV is needed to compensate various ambient forces, including atmospheric drag, radiation pressure, etc. Such orbital maintenance of the satellite (for instance a GEO communication satellite) requires $\Delta V \sim 0.6\,\mathrm{km\,s^{-1}}$ for a 10-year period. The ΔV of deep-space missions are typically several $\mathrm{km\,s^{-1}}$, and a ΔV for an orbit transfer is about a few $\mathrm{km\,s^{-1}}$.

Many types of plasma thrusters have been developed over last 60 years. The variety of these devices can be divided into three main categories dependent on the mechanism of acceleration [1]: (i) electrothermal, (ii) electrostatic and (iii) electromagnetic.

(i) Electrothermal thrusters employ electric energy to heat propellant. In this case the acceleration mechanism

is based on the pressure gradient, which is the same acceleration mechanism as the one employed in chemical thrusters.

(ii) Electrostatic thrusters directly employ an electric field to accelerate ions.

(iii) Electromagnetic thrusters wherein combination of both electric and magnetic fields are employed to accelerate the propellant.

Recent trends in space exploration associate with the paradigm shift towards small and efficient satellites, or micro- and nano-satellites. There are many near-future space missions involving science, military, and commercial payloads utilizing micro- and nano-satellite platforms. These platforms require very small levels of thrust for very fine attitude control, for high resolution Earth imaging and astronomy, and very fine positioning requirements, for spacecraft formation flying and interferometry missions. Nowadays many basic components of a spacecraft are being miniaturized allowing micro-satellites and nano-satellites to be designed and built. To satisfy the needs of both the low-thrust missions and the small-scale spacecraft, miniaturized propulsion systems are required.

It should be pointed out that this paper does not attempt to address the entire field of micropropulsion in detail, but rather describe major issues associated with plasma microthrusters. Some of the mature micropropulsion concepts were described in a recent review article [2]. Broader view of electric propulsion can be found in several dedicated books by Jahn [3], Jahn and Choueiri [4], Goebel and Katz [5], and a special issue of *IEEE Transactions of Plasma Science* (vol 36, issue 5, part 1,2008) [6].

The rest of this paper will be organized as follows. In section 2 we will overview various micropropulsion concepts. In section 3 we will describe in detail one particular example of microthruster, the micro-cathode arc thruster.

2. Plasma-based micropropulsion

Micropropulsion devices producing micro-Newton levels of thrust or micro-Newton-second impulse bits are currently under development in many academic, government and industrial laboratories, and yet the field of micropropulsion is still in its infancy [7]. Recall that the most important issue for microthrusters is propellant management and as such issues related to propellant become critical. In the next section we describe various propulsion concepts and we adopt natural division based on the propellant mechanism. In general, ablative thrusters are the simplest devices in terms of functionality and in fact were the first to be flown in space.

2.1. Ablative pulsed plasma thruster

Ablative pulsed plasma thrusters (PPTs) have achieved a high degree of maturity over several decades of research and development, and flight. The first flight of a PPT took place on the Russian Zond 2 spacecraft in 1964. Subsequent flights took place in the US on the geosynchronous MIT Lincoln Lab LES-6 satellite in 1968, 1974 and the US Navy TIP/NOVA satellite in 1981.

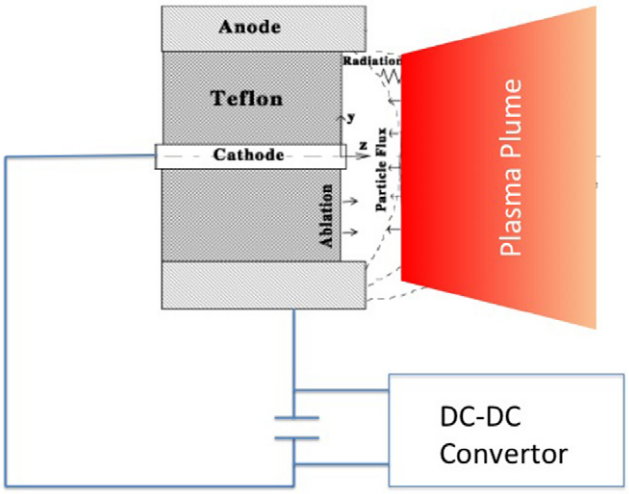

Figure 1. Schematic of the co-axial micro-PPT.

PPTs are currently considered an attractive propulsion option for mass and power limited satellites that require μN s to mN s impulse bits [8–13], One of the most extensively analyzed propulsion functions has been attitude control. For missions that require precision pointing, the PPT offers a unique advantage over other technologies as it delivers a small impulse 'bit' with high specific impulse (exhaust velocity). Another major functional area is station-keeping, which includes drag compensation and formation flying. These functions require less than 1 mN of thrust. For instance, interferometer missions [7] such as ST-3 require sub-millimeter relative positioning precision. An electromagnetic PPT was successfully operated for pitch axis control on the EO-1 spacecraft [14, 15]. It was shown that PPT can be easily scaled down in power and size. A micro-PPT (μPPT) is the miniature version of the traditional PPT, and has been designed at the Air Force Research Laboratory (AFRL) for delivery of very small impulse bits [16, 17]. AFRL μPPT was developed for a demonstration mission on TechSat21 [18] and was recently employed at FalconSatIII. The μPPT can deliver a thrust in the 10 μN range to provide attitude control and station-keeping for micro-satellites.

With the μPPT, the discharge across the propellant surface ablates a portion of the propellant, ionizes it, and then accelerates it predominantly electromagnetically to generate the thrust (schematically this thruster is shown in figure 1) [19, 20]. It is expected that the use of electromagnetic acceleration to create thrust will also lead to relatively high specific impulse.

Recall that both discharge energy (peak current) and thruster size significantly affect the discharge uniformity in the azimuthal and radial directions. Azimuthal non-uniformity relates to the current constriction and anode spot formation phenomena. This effect occurs when the discharge current or thruster size exceed some critical value. Non-uniformity in discharge associated with the spot mode leads to a much higher localized ablation rate and causes degradation of the specific impulse. On the other hand, small discharge current leads to strong Teflon surface carbonization (charring) and

radial non-uniformity, which in turn leads to thruster failure [20]. The primary mechanism of the charring formation was identified and is related to carbon backflux. Thruster size and discharge energy can be optimized by trading between two conflicting requirements of large pulse energy (to prevent charring) and small discharge energy (to prevent current constriction) [21]. Because the charring phenomenon is completely intolerable and leads to thruster failure, the optimal discharge energy should be chosen somewhere near the spot formation limit.

2.2. Micro-laser plasma thruster

Another good example of the ablative type of micro-propulsion system is the micro-laser-ablation plasma thruster (μ-LPT). Some variations of this device have been developed by Phipps and Luke [22] and Gonzalez and Baker [23]. In [22] a Q-switched micro-chip laser, pumped by a cw diode laser, was used to ablate an aluminum target generating thrust in the range of 0.3 nN to 3 μN with power consumption of about 5 W and pulse frequency in the range of 1 Hz to 10 kHz. The wide dynamic range of thrust levels provided by these devices is one of their most attractive features.

The micro-Laser-Ablation Plasma Thruster (μ-LPT) developed by Phipps and Luke [22] uses a 1–10 W, high-brightness diode laser irradiating various absorbing material and substrate combinations (e.g. black ink on paper, black PVC on Kapton^{TM}). Laser coupling coefficients on the order of 60 μN W^{-1} and specific impulses on the order of 500 s with a 1 W laser are achieved. One of the major advantages of the μ-LPT is its large dynamic range of impulse bit that can be varied between 0.4 to 16 μN s by simply increasing the laser pulse duration. In addition, selection of the absorber and substrate materials allows the specific impulse and laser characteristics to be tailored for specific mission requirements.

The μ-LPT can be operated in two different modes. In reflection mode (R), the laser is incident on the target and the ablated material 'reflects' from the surface. This mode has the potential problem of leading to deposition of plume effluent on the laser optics. In transmission mode (T), the laser passes through a transparent substrate film from the back. The substrate is coated on the other side with an absorbing material that ablates material away from the laser. This approach circumvents the problem of optics contamination found with the R-mode. However, the dynamic range of impulse bit available in T-mode is more restrictive. Coating of the laser optics by plume deposition is one of the major lifetime limitations of the μ-LPT in R-mode. Therefore, there is a certain preference for development of T-mode operation. Computational analysis of the R-mode μ-LPT was performed using hybrid particle-in-cell technique [24]. A lens focuses the laser diode output on a 25 μm diameter spot on the transparent side of a fuel tape. The beam heats an absorbing coating to high temperature, producing a miniature ablation jet. The material that is ablated is usually PVC or Kapton^{TM}. Typical parameters of operation are: power of 2 to 14 W, pulse duration of 3–10 ms. The fuel tape thickness is about 185 μm, composed of 125 μm of transparent backing (usually cellulose acetate) and about 60 μm of absorbing coating. Typically Q^* (energy of laser light required to ablate 1 kg of target material) is about 2×10^7 J kg^{-1} and the momentum coupling coefficient is about $C_w = 60 - 100\,\mu$N W^{-1}. Computational analysis of the T-mode μ-LPT was also developed and compared with an experiment [25]. Generally the LPT models have satisfactorily described the main features of the thruster, such as ablated mass and plume expansion.

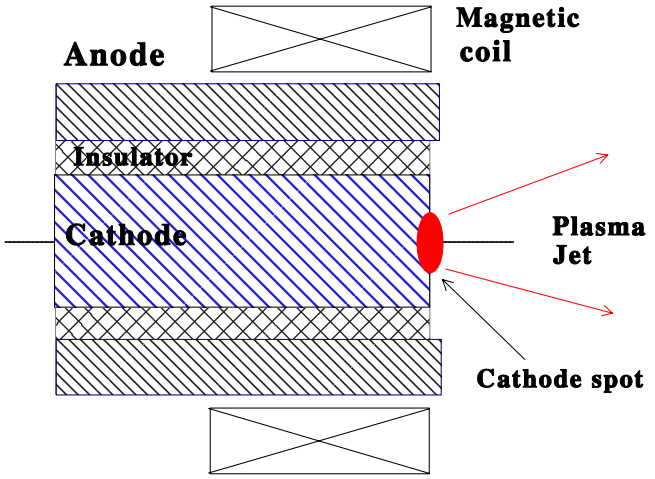

Figure 2. Schematics of the vacuum arc thruster (reproduced with permission from [32]).

2.3. Micro-vacuum arc thruster

One possibility to improve some aspects of PPTs without compromising its efficiency is to use metal as a propellant. Recent success in the development of vacuum arc technology has attracted much attention to this technology [26]. Metal propellant will have the following benefits: lower energy consumption per mass ionized (due to the low ionization potential of metals), high ionization degree, operation with higher repetition rates since the metal melting temperature is higher than that of polymer dielectrics used in some current thrusters, and high pulse-to-pulse stability. For these reasons a vacuum arc source was developed and used for an ion thruster [27]. This work led to development of a co-axial vacuum arc plasma thruster [28]. Schematically this thruster is shown in figure 2. However, the measured efficiency was reported to be only ~1.6% which is strongly different from the estimations, leaving ample room for improvement. On the other hand several problems related to this technology were reported, including lifetime, ion current degradation with cathode recession, etc [29]. Therefore understanding these problems and the efficiency limitations of the vacuum arc thruster technology is an important issue. In addition, basic aspects of vacuum arc thrusters such as thrust mechanism, effects of the magnetic field of the thruster operation and its plume, and droplet generation were not studied in detail. Very recently it was shown that using an axial magnetic field (so-called magnetically enhanced vacuum arc thruster) helps to improve thruster characteristics, such as specific impulse (plasma velocity) and decrease plasma plume divergence [30, 31].

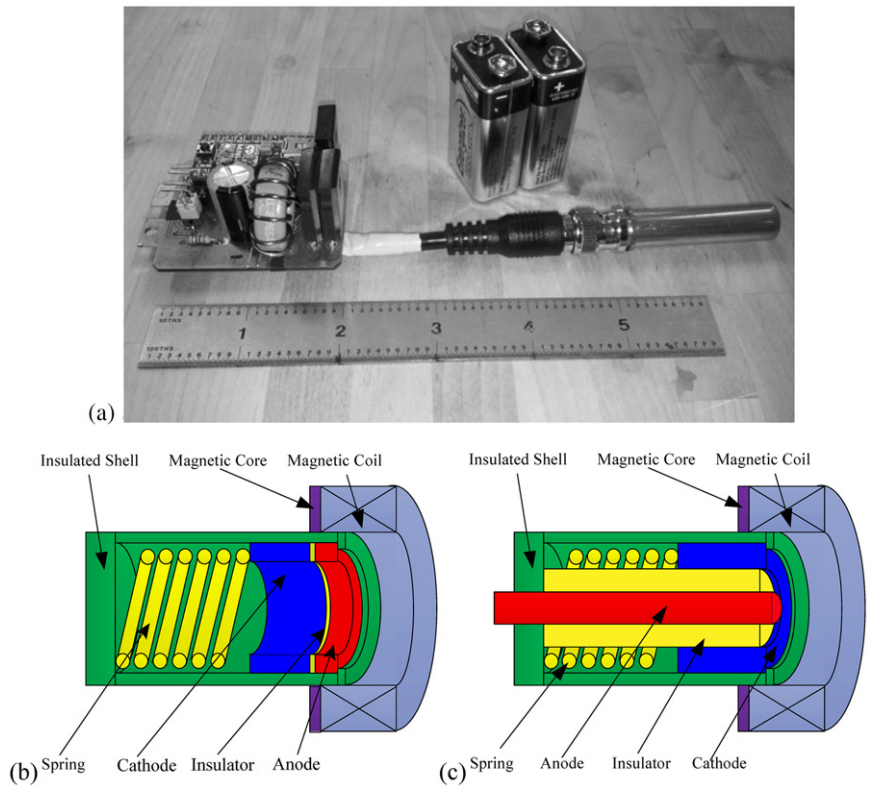

Figure 3. (*a*) μCAT with PPU. (*b*) Schematic design of the ring shape μCAT, (*c*) schematic design of co-axial electrodes μCAT.

With the vacuum arc thruster the thrust is created in the minute spot on the cathode surface called cathode spots (having size of about 10–100 μm) [32]. The high-pressure plasma in the cathode spot creates the reaction force (thrust) on the cathode as schematically shown in figure 2. As earlier as in the 1930s it was found experimentally that the plasma stream exerts a reaction force on the cathode, which is about 17 ± 3 dyn A^{-1} (or $\sim$0.2 mN A^{-1}) [33, 34]. It is very important to note that since the reaction force is proportional to the arc current, the thrust can be controlled relatively easily.

3. Micro-cathode arc thruster

Recently, a new thruster configuration, the micro-cathode arc thruster (μCAT), was developed motivated by need for an efficient low mass propulsion system. This thruster improves on the vacuum arc discharge thruster by applying a specially designed external magnetic field. The unique magnetic field conditions achieved with a vacuum arc offer several potential advantages in these devices [35].

The μCAT is a simple electric propulsion device and combined with a magnetic coil and an inductive energy storage power processing unit (PPU) results in a low mass (<100 g) system. A picture of the μCAT system and two types of geometries of a thruster are shown in figures 3(*a*)–(*c*). Figure 3(*b*) shows the schematic design of the ring electrodes μCAT (RE-μCAT), which consist of an annular titanium cathode and a same diameter annular copper anode with 1 mm width. The annular ceramic insulator tube having same inner and outer diameters and a width of about 1 mm was used as separator between the arc electrodes. Figure 3(*c*) shows the schematic design of the co-axial μCAT. Instead of the ring electrodes, this design employs cylindrically shaped cathode and anode.

Figure 4(*a*) presents a schematic of the thruster and the PPU system. The PPU that has been designed is equipped with an inductive energy storage system as shown in figures 4(*a*) and (*b*). When the trigger pulse is applied to a semiconductor insulated gate bipolar transistor (IGBT) switch, the energy is accumulated in the inductor, while when the trigger pulse ends; a surge voltage with the magnitude proportional to $L\,\mathrm{d}I/\mathrm{d}t$ is generated on the inductor and applied to the electrodes. This leads to a breakdown and initiation of arc discharge between the electrodes. A coil has been applied to the outside of the thruster to produce magnetic field as indicated in figure 4(*a*). The field strength was simulated using Finite Element Method Magnetics (FEMM) magnetic field simulation software. The direction of the magnetic field could be simply reversed by reversing the coil current.

The μCAT operates by producing a fully ionized plasma at the inner surface of the electrode. The plasma is formed in the cathode spots, and expands into the vacuum zone under the applied magnetic field gradient. The plasma then accelerates and expands into vacuum at high velocities, around tens of thousands m s^{-1}, which results in an impulse bit. The effect of the magnetic field on the thruster operation is clearly visible in figure 4(*b*). This figure shows a CCD camera observation of the RE μCAT firing in the vacuum chamber with an added magnetic field ($B = 0.3$ T) and without.

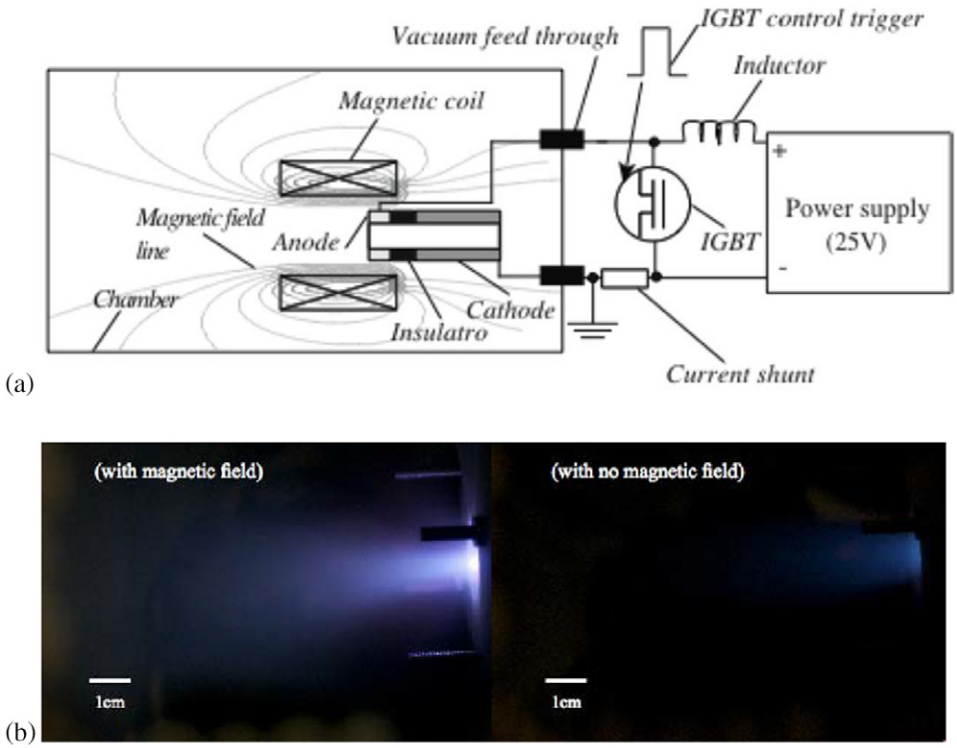

Figure 4. (*a*) Schematic of micro-cathode vacuum arc thruster experimental arrangement. (*b*) CCD camera observation of plasma plume with magnetic field (left image, $B = 300$ mT) and with no magnetic field.

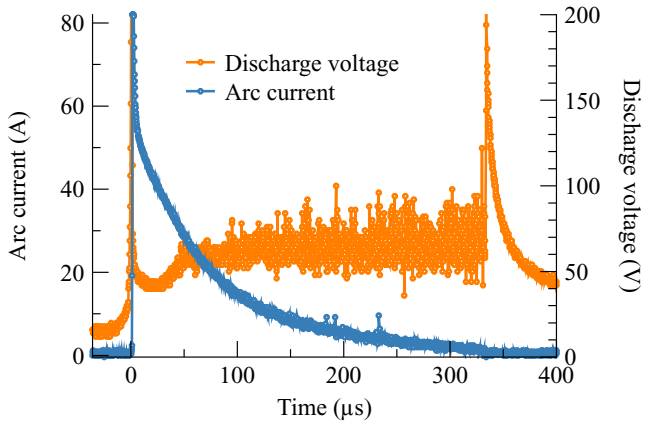

Figure 5. Evolution of μCAT arc current (blue line) and discharge voltage (yellow line) in the case of a magnetic field of about 100 mT.

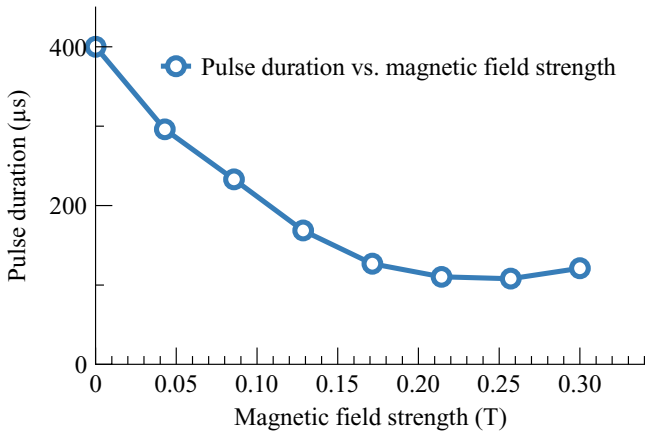

Figure 6. Thruster pulse duration evolution with different magnetic field strength.

3.1. Experimental characterization of the micro-CAT

The arc voltage during the discharge process remains approximately constant, yet it is found that this constant voltage varies with the magnetic field strength. A typical sample of μCAT arc current and discharge voltage evolution is indicated in magnetic field strength of about 100 mT. Typically, during the discharge process, the current that was flowing through the solid-state switch is fully transferred to the cathode spots, as indicated in the figure 5. Consequently, the current dropped down from around 80–100 A to 0 A (for around 100–400 μs varied with magnetic field strength as shown in figure 5). Pulse duration is also affected by a magnetic field as shown in figure 6. A previous work of Keidar *et al* [32] indicated that an axial magnetic field located near the anode region plays an important role, and indicated that the arc voltage increases when a magnetic field is applied. The experimental results agree well with the theoretical predication.

The plasma formed by a vacuum arc is created on the cathode surface spots. Previously optical method were employed and it was observed that the spot consists of either a homogeneous bright region or consists of cells and fragments with a typical total size of about 10–100 μm [36, 37]. The μCAT is equipped with a coil that provides magnetic field strength in the range of 0–300 mT. The observation of cathode spot motion under magnetic field was first studied in the

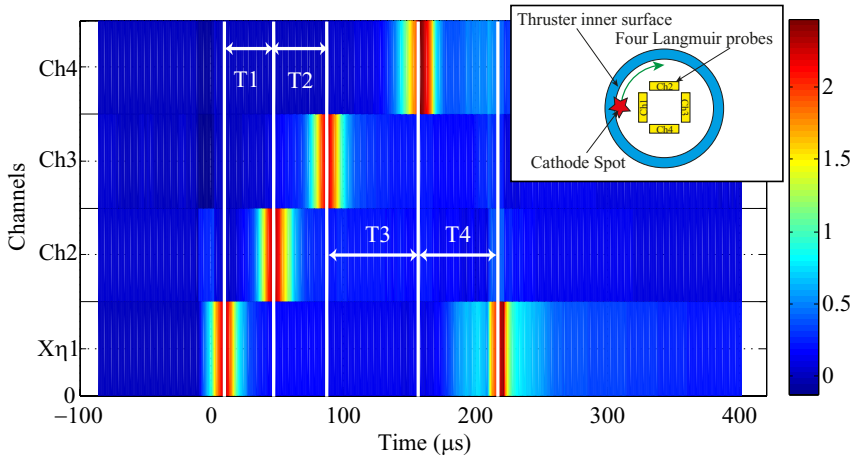

Figure 7. Example of four Langmuir probes method to measure the cathode spot rotation speed.

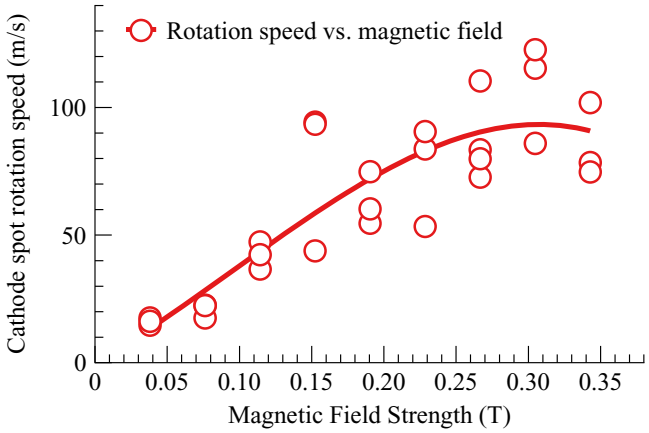

Figure 8. Distribution of μCAT cathode spot rotation speed with different magnetic field strengths [40].

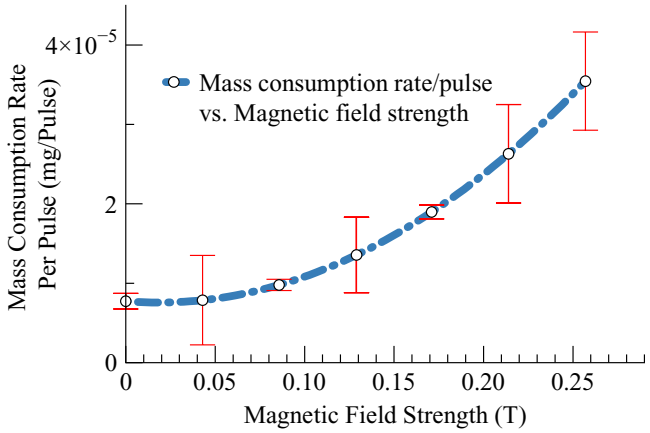

Figure 9. Thruster cathode material erosion rate with different magnetic field strength.

1960s [38, 39]. It is known that the presence of a transverse magnetic field at the cathode surface produces arc rotation in the $-J \times B$ direction. The observed vacuum arc cathode spot rotation has important implications for propulsion. The benefits are observable in that the cathode spot rotation leads to uniform cathode erosion, which is critical for assuring long thruster lifetime. The μCAT cathode spot rotation could be measured by utilizing 4-probe assembly of Langmuir probes. Four single probes were located along the azimuth direction inside the thruster channel, and the four probes ion current measurement results are shown in figure 7. The rotation speed was calculated using a quarter of circumference of the thruster's inner surface, divided by the delay time between each two neighbor peaks. The average rotation speed is shown in figure 8. It was found that the spot rotation speed increased about 5 times (from 20 to 100 m s^{-1}) as the magnet field strength increased (from 0 to 300 mT). More detailed descriptions of this effect can be found in [40].

It was also found that the applied magnetic field increases the thruster erosion rate. In [41] the cathode material erosion rate was reported to increase almost three times when the magnetic field was increased from zero up to 300 mT. The mass consumption rate was measured utilizing a highly accurate mass balance. These results (see figure 9) show that the added magnetic field leads to an increase of mass consumption rate by a factor of 3, from around 1×10^{-5} mg/pulse at zero magnetic field strength to around 3×10^{-5} mg/pulse at 0.25 T magnetic field. There are two reasons for increased mass consumption rate. Firstly, the magnetic field contributes to the transport of the metal plasma out of the thruster channel. Secondly, the rotation of cathode spots promotes erosion efficiency by moving the spot over a larger area of the thruster cathode.

3.2. μCAT plume characterization

In this section we present a 2D spatial and temporal evolution of the plasma plume outside the thruster channel in the presence of an applied magnetic field. The two-dimensional analysis of plasma flow affected by an externally imposed magnetic field was performed by Keidar and co-workers [42–44]. The experimental measurement of μCAT plasma flow was done in [45]. In that work, the spatial distribution of plasma was obtained using a set of axially aligned circular Langmuir probes. Each probe consisted of eight concentric circular planar probes separated by an insulating ring that were aligned with the thruster axis. Figure 10 presents the 2D ion current maps for different magnetic field strengths. One can see that

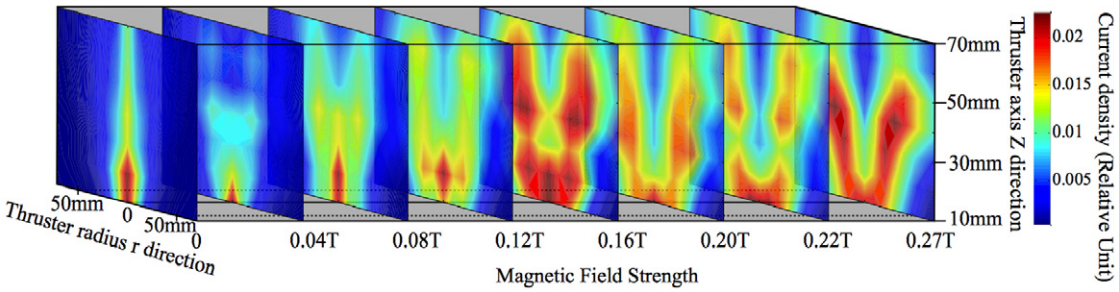

Figure 10. D spatial distribution of ion current with different magnetic field.

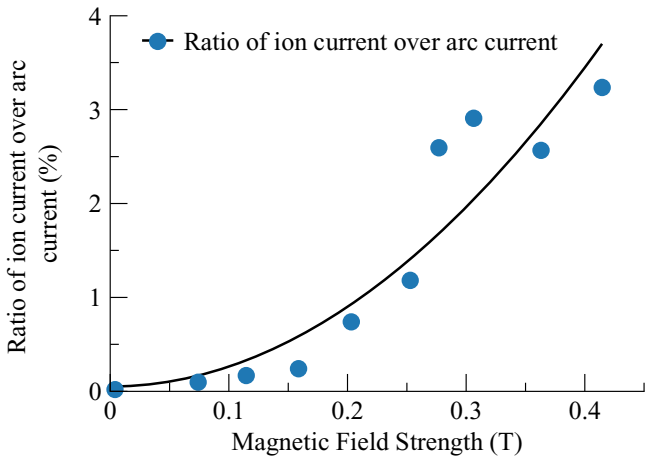

Figure 11. The ratio of thruster total ion current over the arc current with different magnetic field.

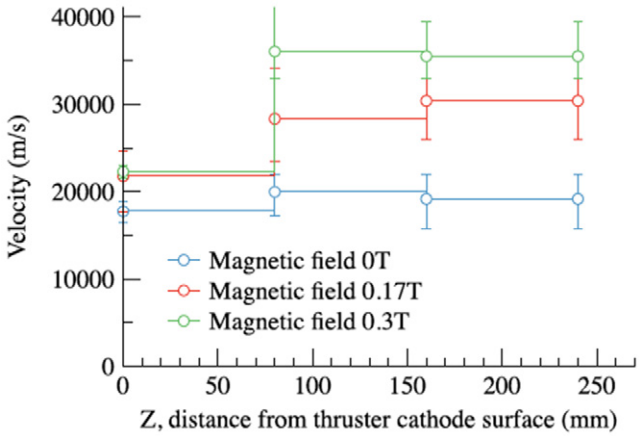

Figure 12. Measured ion velocity along the axis with magnetic field as a parameter. Reprinted with permission from [47]. Copyright 2011, AIP Publishing LLC.

magnetic field leads to a plasma collimation along magnetic field lines as shown in figure 10. In addition, one can notice the hollow shape of the plasma plume consequent by increasing the magnetic field strength. It can be noticed that the external magnetic field of the μCAT leads to an improvement of plasma plume transport efficiency along the magnetic field.

The total ion beam current in the plume is a critical parameter needed to evaluate the thruster efficiency. It is well known that in the case of Ti cathode the maximum ratio of ion current over arc current is about 8% [46]. As indicated in [45], the measured μCAT total ion current output with no magnetic field is about 0.06%, yet, when the magnetic field is applied the aforementioned efficiency increases up to 3.5%, as shown in figure 11. This translates into approximately 45% of transport efficiency.

3.3. Ion velocity in micro-CAT

In this section we will discuss the ion acceleration mechanism in the μCAT. Recall that based on our measurements [47] one can identify three characteristics regions. Approximately up to 80 mm from the cathode is the interelectrode region, in which plasma is being produced and accelerated by a pressure gradient due to electron–ion coupling, i.e. by the gas dynamic mechanism. It should be pointed out that the ion velocity close to the arc source is independent of the magnetic field, which demonstrates that the magnetic field strength utilized in our experiments does not significantly affect the gas dynamic acceleration of ions in vicinity of the cathode spot. The second region, which is about 80–150 mm from the cathode surface is the plasma expansion inside and outside the thruster, where ion acceleration in a magnetic field was observed as shown in figure 12. Let us consider a possible mechanism of plasma acceleration in this region. Plasma flow is subject to the electromagnetic force in the divergent magnetic field region:

$$Mn\frac{\mathrm{d}V}{\mathrm{d}t} = j_\theta B_r \tag{1}$$

where M is the ion mass, n is the plasma density, j_θ is the azimuthal electron current and B_r is the radial component of the magnetic field. One can estimate the azimuthal electron current density as

$$j_\theta = \frac{\omega_\mathrm{e}}{\nu_\mathrm{ei}} j_r \tag{2}$$

where j_r is the electron radial current density. In the plasma jet outside of the interelectrode gap, the global current is zero so that the electron current is equal to the ion current. Thus

$$j_{er} = j_{ir} = enV_r \tag{3}$$

where V_r is the radial component of the ion current. The radial component of the plasma is developed in course of the plasma expansion [42] and could be about 0.3 of the axial component in a large magnetic field.

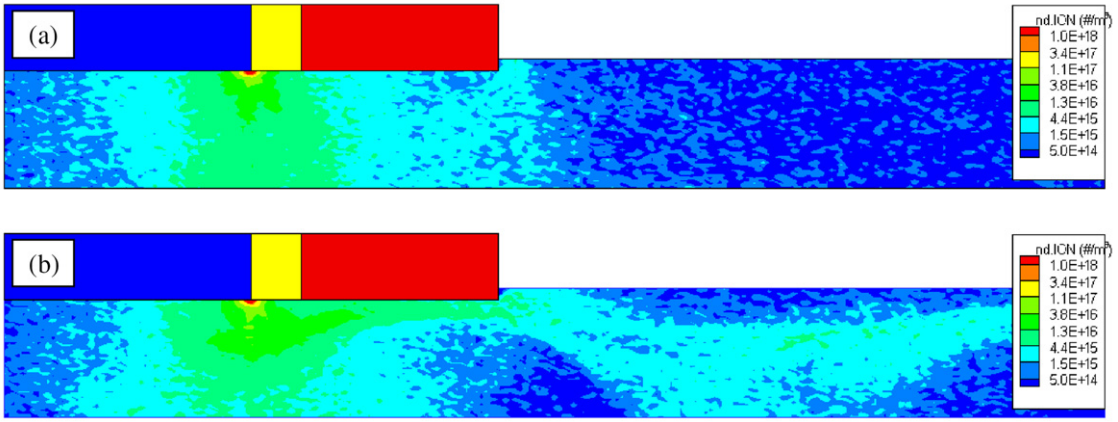

Figure 13. Comparison of ion density without (a) and with (b) the applied magnetic field. Thruster components correspond to the figure 3.

Based on the above scenario one can estimate the ion velocity change in the axial direction as

$$\Delta V_z \approx \sqrt{\frac{2e^2 B_z B_r V_r \Delta z}{m M \nu_{ei}}}. \quad (4)$$

Using the following typical parameters of the plasma jet: B (i.e. both B_r and B_z) ~ 0.1 T, $n \sim 10^{20}$ m^{-3}, $V_r \sim 10^4$ m s^{-1} and $\Delta z \sim 0.01$ m one can estimate that $\Delta V_z \sim 10^4$ m s^{-1}. One can point out that these results are in good agreement with experimental measurements.

It should be pointed out that cathodic arc plasmas include macroparticles generated in the cathode spot [46]. The size and density of macroparticles depend on the cathode material and arc operation [46]. Typically these are 1–10 μm in diameter spherical droplets [48]. Presence of macroparticle in the plume might raise a concern with respect to thruster contamination. However, it should be pointed out that macroparticle emission generally decreases in the case of a pulsed arc in comparison with dc vacuum arc. In addition, emitted macroparticles interact with high-velocity plasma jet and momentum transfer between plasma and macroparticle leads to macroparticle emission in the direction of jet propagation [49], i.e. away from the satellite. Since no backflux was determined in the case of micro-CAT one can expect no macroparticle backflux and as such negligible contamination risk.

3.4. Simulation of the μCAT

We have also completed an initial numerical analysis of the thruster. The primary goal of this investigation was to demonstrate the feasibility of the numerical approach. We were interested in determining whether a fully-kinetic approach, in which both electrons and ions are treated as particles, is suitable for modeling the turning of the ion beam, and the increased ion velocity observed experimentally. Various kinetic codes were developed for application in electric propulsion [50–52]. As such, we set up the simulation using the 3D electrostatic particle-in-cell code Draco [53]. In this work, two cases are considered. The first case did not contain any magnetic field. In the second case, the background magnetic field was loaded, corresponding to coil current of 0.4 A. In this configuration, the magnetic field lines form an angle of approximately 15° from the cathode surface at the location of the cathode spot. Since Draco is a 3D code, the axisymmetric geometry is represented by modeling a thin slab, in which the periodic boundary condition was applied to the front and back faces. The simulation domain can be seen in figure 13. The cathode is shown by the orange rectangle. The gray rectangle is the insulator, and the blue shape is the anode. Potential difference of 50 V was applied between the electrodes. Electrons and ions were injected from a small control surface located at the junction of the cathode and the insulator, at flow rates corresponding to 0.4 A. We assumed that the beam consisted solely of electrons and doubly charged Ti^{2+} ions [54]. Neutral particles were not modeled directly, but instead we loaded a constant background density corresponding to 6×10^{-5} Torr. Collisions were included through the Monte Carlo collisions (MCC) scheme with cross-sections determined from analytical models. Momentum transfer and Coulomb collisions were considered. The simulation contained $10 \times 50 \times 226$ cells, and approximately 2 million particles. No artificial scaling of permittivity was performed. Figures 13(a) and 13 (b) show the preliminary results. Comparison of these figures clearly illustrates the influence of the magnetic field. In figure 13(a), in which there is no magnetic field, the ions are seen to simply diffuse out from the cathode spot. No significant thrust is expected to be generated in this configuration. However, the addition of the magnetic field, figure 13(b), clearly shows the extraction of the ion beam from the thruster as demonstrated experimentally. Although not shown here, the simulation results presented in figure 13(b) indicate that with adding a magnetic field, the ion velocity reaches the magnitude of 4×10^4 m s^{-1} which agrees with the experimental results.

3.5. Comments on comparison of micropropulsion technologies

The comparison of micropropulsion technologies operating in the low powers range of <10 W is presented in table 1. Utilization of metal propellant allows the μCAT system to carry larger amounts of propellant in smaller volume in comparison with ion thruster and PPT, which utilize gas and

Table 1. Comparison of micropropulsion technologies.

	μCAT (GWU)	PPT (Clyde Space) [55, 56]	PPT (Busek Co) [57–59]	Electrospray (MIT) [60–62]	Electrospray (Busek Co) [57, 58]	VAT (Alameda) [63]
System mass (g)	200	160	550	45	1150	600
System volume (cm^3)	200	200	500	300	500	200
Propellant	Metal	Teflon	Teflon	Liquid	Liquid	Metal
I_{sp} (s)	3000	590	700	3000	800	1500
Propellant mass (g)	40	10	36	20	75	40
Delta-V (for 4 kg satellite) ($m\,s^{-1}$)	300	15	63	150	151	151
Efficiency (%)	15	4.7	16	71	31	9.4
Thrust-to-mass ratio ($\mu N\,g^{-1}$)	0.63	0.03	0.18	0.5	0.65	0.22
Ionization degree	High	Low	Low	High	High	High
Cost	Low	Low	Low	High	High	Low
Technical readiness level (TRL)	6	7	7	2–3	5	4

Teflon propellants respectively. It is seen that the μCAT subsystem has mass and volume characteristics comparable or exceeding that of other micropropulsion technologies. In addition, the μCAT is providing the highest I_{sp} of about 3500 s, due to the high speed of the plasma produced by the cathodic arc. Both of these factors (large amount of carried propellant and high I_{sp}) ensures leadership of μCAT technology in the Delta-V parameter. The μCAT is characterized by an ionization degree close to 100% in the plasma jets in comparison with several tens of percent for PPT and ion thruster technologies. Low ionization degree is a critical issue, since it causes strong back flux to a satellite and results in contamination issues. Finally, μCAT technology is characterized by very high overall efficiency and thrust-to-mass ratio in comparison with competing technologies.

4. Concluding remarks

In this paper, a comprehensive characterization of the μCAT has been presented. It has been found that the thruster with different magnetic strength exhibits certain regularities in its behavior, which has been observed through experimental measurements. The cathode spot motion was observed and results indicated that the magnetic field leads to cathode spot rotation which is critical for uniform cathode erosion. The plasma plume distribution outside the thruster channel has been presented to analyze the effects of the magnetic field on the plasma plume. A preliminary numerical analysis of the thruster has also been completed, with the simulation results confirming the ion extraction effect of the magnetic field. The μCAT equipped with a magnetic field operates efficiently and gives great flexibility in specific impulse and impulse bit by simply varying the magnetic field strength.

Acknowledgment

This work was supported in part by NASA DC grant.

References

[1] Choueiri E Y 2007 Plasma Propulsion *McGraw-Hill Encyclopedia of Science and Technology* (New York: McGraw-Hill)
[2] Ahedo E 2011 *Plasma Phys. Control. Fusion* **53** 124037
[3] Jahn R 1968 *Physics of Electric Propulsion* (New York: McGraw-Hill)
[4] Jahn R and Choueiri E 2002 Electric propulsion *Encyclopedia of Physical Science and Technology* (New York: Academic) pp 125–41
[5] Goebel D and Katz I 2008 *Fundamentals of Electric Propulsion: Ion and Hall Thrusters* (New York: Wiley)
[6] Keidar M, Gallimore A D, Raitses Y and Bouef J P (ed) 2008 Special Issue on Plasma Propulsion *IEEE Trans. Plasma Science* **36** 1962–6
[7] Keidar M and Beilis I I 2013 *Plasma Engineering: Applications from Aerospace to Bio and Nanotechnology* (New York: Academic)
[8] Spores R A, Cohen R B and Birkan M 1997 The USAF electric propulsion program *Proc. 25th Int. Electric Propulsion Conf. (Worthington, OH, 1997)* vol 1, p 1
[9] Micci M M and Ketsdever A D (ed) 2000 *Micropropulsion for Small Spacecraft* (Reston, VA : AIAA)
[10] Burton R L and Turchi P J 1998 Pulsed plasma thruster *J. Propulsion Power* **14** 716–35
[11] Scharlemann C A, Corey R, Mikellides I G, Turchi P J and Mikellides P G 2000 Pulsed plasma thruster variations for improved mission capabilities *AIAA Paper*-00-3260
[12] Choueiri E Y 1996 System optimization of ablative pulsed plasma thruster for stationkeeping *J. Spacecraft Rockets* **33** 96–100
[13] Keidar M and Boyd I D 2000 Device and plume model for an electrothermal pulsed plasma thruster *AIAA Paper* 2000–3430
[14] Dunning J W, Benson S and Oleson S 2001 NASA's electric propulsion program *27th Int. Electric Propulsion Conf. (Pasadena, CA, October 2001)* IEPC-01-002
[15] Zakrzwsky C, Benson S, Sanneman P and Hoskins A 2002 On-orbit testing of the EO-1 pulsed plasma thruster *38th Joint Propulsion Conf. (Indianapolis, IN, July 2002)* AIAA-2002-3973
[16] Spanjers G G, White D, Schilling J, Bushman S, Lake J and Dulligan M 2001 AFRL microPPT development for the TechSat21 flight *27th Int. Electric Propulsion Conf. (Pasadena, CA 2001)* IEPC Paper 2001-166

[17] Spanjers G G *et al* 2002 AFRL microPPT development for small spacecraft propulsion *38th AIAA Joint Propulsion Conf. (Indianapolis, IN, July 2002)* Paper AIAA-2002-3974

[18] Gulchinski F S *et al* 2000 Micropropulsion research at AFRL *36th AIAA Joint Propulsion Conf. (Huntsville, AL, July 2000)* Paper AIAA-2000-3255

[19] Keidar M, Boyd I D and Beilis I I 2003 Model of an electrothermal pulsed plasma thruster *J. Propulsion Power* **19** 424–30

[20] Keidar M, Boyd I D, Antonsen E L, Gulczinski F S III and Spanjers G G, Propellant charring in pulsed plasma thrusters 2004 *J. Propulsion Power* **20** 978

[21] Keidar M, Boyd I D, Antonsen E L, Burton R L and Spanjers G G 2006 Optimization issues for a micro-pulsed plasma thruster *J. Propulsion Power* **22** 48–55

[22] Phipps C and Luke J 2002 Diode laser-driven microthrusters: a new departure for micropropulsion *AIAA J.* **40** 310–17

[23] Gonzalez D A and Baker R P 2001 Microchip laser propulsion for small satellites *37th AIAA/ASME/SAE/ASEE Joint Propulsion Conf. (Salt Lake City, UT, USA, July 2001) AIAA Paper* 2001-3789

[24] Boyd I D and Keidar M 2002 Simulation of the plume generated by a micro laser-ablation plasma thruster *High-Power Laser Ablation IV* ed C R Phipps *Proc. SPIE* **4760** 852

[25] Keidar M, Boyd I D, Luke J and Phipps C 2004 Plasma generation and plume expansion for a transmission-mode micro-laser plasma thruster *J. Appl. Phys.* **96** 49–56

[26] Polk J *et al* 2001 A theoretical analysis of vacuum arc thruster performance *IEPC Paper* IEPC-2001-211

[27] Qi N, Gensler S, Prasad R R, Krishnan M, Visir A and Brown I G 1998 A pulsed vacuum arc ion thruster for distributed small satellite systems *AIAA Paper* AIAA-98-3663

[28] Qi N, Schein J, Binder R, Krishnan M, Anders A and Polk J 2001 *37th Joint Propulsion Conf. (Salt Lake City, UT, 8–11 July 2001)*

[29] Schein J, Qi N, Binder R, Krishnan M, Ziemer J K, Polk J E and Anders A 2001 Low mass vacuum arc thruster system for station keeping missions *IEPC Paper* 01-228

[30] Au M, Schein J, Gerhan A, Wilson K, Tang B and Krishnan M 2004 *AIAA Paper* 2004-3618

[31] Keidar M and Schein J 2004 Modeling of a magnetically enhanced vacuum arc thruster *40th AIAA Joint Propulsion Conf. (Fort Lauderdale, FL, July 2004)* Paper AIAA-04-4117

[32] Keidar M, Schein J, Wilson K, Gerhan A, Au M, Tang B, Idzkowski L, Krishnan M and Beilis I I 2005 Magnetically enhanced vacuum arc thruster *Plasma Sources Sci. Technol.* **14** 661–9

[33] Tanberg R 1930 *Phys. Rev* **35** 1080

[34] Robertson R 1938 *Phys. Rev.* **53** 578

[35] Beilis I I 2002 *IEEE Trans. Plasma Sci.* **30** 2124–32

[36] Djakov B E and Holmes R 1974 *J. Phys. D: Appl. Phys.* **7** 569

[37] Juttner B 2001 *J. Phys. D: Appl. Phys.* **34** R103

[38] Murphree D 1970 *Phys. Fluids* **13** 1747

[39] Ecker G and Muller K G 1958 *J. Appl. Phys.* **29**1606

[40] Zhuang T, Shashurin A, Keidar M and Beilis I I 2011 Circular periodic motion of plasma produced by a small-scale vacuum arc *Plasma Sources Sci. Technol.* **20** 015009

[41] Zhuang T, Shashurin A, Denz T, Vail P, Pancotti A and Keidar M 2014 Performance characteristics of micro-cathode arc thruster *J. Propulsion Power* **30** 29–34

[42] Keidar M, Beilis I I, Boxman R L and Goldsmith S 1996 *J. Phys. D: Appl. Phys.* **29** 1973–83

[43] Beilis I, Keidar M, Boxman R L and Goldsmith S 1998 *J. Appl. Phys.* **83** 709–17

[44] Keidar M, Beilis I, Boxman R L and Goldsmith S 1997 *IEEE Trans. Plasma Sci.* **25** 580–5

[45] Zhuang T, Shashurin A and Keidar M 2011 *IEEE Trans. Plasma Sci.* **39** 2936–7

[46] Boxman R L, Martin P J and Sanders D M 1995 *Vacuum Arc Science and Technology* (Park Ridge, NJ: Noyes)

[47] Zhuang T, Shashurin A, Beilis I and Keidar M 2011 Ion velocities in a micro-cathode arc thruster *Phys. Plasmas* **19** 063501

[48] Keidar M, Beilis I, Boxman R L and Goldsmith S 1995 Non-stationary macroparticle charging in an arc plasma jet *IEEE Trans. Plasma Sci.* **23** 902–8

[49] Keidar M, Beilis I, Boxman R L and Goldsmith S 1996 Transport of macroparticles in magnetized plasma ducts *IEEE Trans. Plasma Sci.* **24** 226–34

[50] Taccogna F *et al* 2008 *Plasma Sources Sci. Technol.* **17** 024003

[51] Szabo J *et al* 2014 *J. Propulsion Power* **30** 197

[52] Kalentev *et al* 2014 *Contrib. Plasma Phys.* **54** 235

[53] Brieda L, Pierru J, Kafafy R and Wang J 2004 Development of the Draco code for modeling electric propulsion plume interactions *40th Joint Propulsion Conf. (Fort Lauderdale, FL, 2004)* AIAA-2004-3633

[54] Keidar M, Brown I G and Beilis I I 2000 Axial ion charge state distribution in the vacuum arc plasma jet *Rev. Sci. Instrum.* **71** 698–700

[55] Guarducci M and Gabriel S B 2011 Design and testing of a micro pulsed plasma thruster for Cubesat application *32nd Int. Electric Propulsion Conf. (Wiesbaden, Germany, 11–15 September 2011)* IEPC-2011-239

[56] www.clyde-space.com/cubesat_shop/propulsion/303_cubesat-pulse-plasma-thruster

[57] Hruby V 2012 High Is CubeSat propulsion *1st Interplanetary CubeSat Workshop (Massachusetts Institute of Technology, Cambridge, MA, 29–30 May 2012)*

[58] www.busek.com/

[59] Mueller J, Ziemer J, Hofer R, Wirz R and O'Donnell T 2008 A survey of micro-thrust propulsion options for microspacecraft and formation flying missions *Cube Sat—5th Annual Developers Workshop (California Polytechnic State University, San Luis Obispo, CA, 9–11 April 2008)*

[60] Martel F and Lozano P 2012 Ion electrospray thruster assemblies for CubeSats *iCubeSat Workshop (Cambridge, MA, 29–30 May 2012)*

[61] Gassend B L P 2007 Fully microfabricated two-dimensional electrospray array with applications to space propulsion *PhD Thesis* Massachusetts Institute for Technology

[62] Velásquez-García L F, Akinwande A I and Martínez-Sánchez M 2006 Planar array of micro-fabricated electrospray emitters for thruster applications *J. Micromech. Syst.* **15** 1272

[63] ww.aasc.net/micropropulsion